This is a postprint version of the published document at:

Rodríguez-Millán, M., Vaz-Romero, Á. y Arias, Á. (2015). Failure behavior of 2024-T3 aluminum under tension-torsion conditions. *Journal of Mechanical Science and Technology*, 29 (11), pp. 4657-4663.

Failure behavior of 2024-T3 aluminum under tension-torsion conditions [†]

Marcos Rodríguez-Millán[1,*], Álvaro Vaz-Romero[2] and Ángel Arias[2]

[1]*Department of Mechanical Engineering, University Carlos III of Madrid, Avda. de la Universidad 30, 28911 Leganés, Madrid, Spain*

[2]*Department of Continuum Mechanics and Structural Analysis, University Carlos III of Madrid, Avda. de la Universidad 30, 28911 Leganés, Madrid, Spain*

Abstract

Experimental and numerical investigations of the failure strain of aeronautical 2024-T3 aluminum were conducted. Experiments on the Double notched tube (DNT) specimen loaded in combined tension and torsion were applied to an aluminum alloy for the first time. Nu-merical analysis showed that the specimen exhibited uniformity in stress-strain as plastic strain developed. Low triaxiality values and a wide range of Lode parameter values were obtained at failure conditions. The failure strain of 2024-T3 aluminum showed strong depend-ence on the Lode parameter in agreement with the observations reported by other authors. The use of the DNT specimen was proven to be efficient in calibrating the ductile failure model of aluminum alloys.

Keywords: Aerospace materials; Aluminum 2024; Failure behavior; Lode parameter; Stress triaxiality

1. Introduction

Aluminum alloys are widely used as structural materials of engineering components. They are applied to aircrafts, wing tension members, truck wheels, scientific instruments, and orthopedic braces, among others, because of their high strength, excellent fatigue resistance, and good strength-to-weight ratio. The most widely used aluminum alloy for the aerospace and aeronautical industries is 2024-T3 alloy. The failure behavior of 2024-T3 alloy is well known under simple stress states. However, engineering applications can be subjected to complex stress states from combined loads. The successful design of mechanical components requires damage models for failure behavior prediction at different loading conditions. For ductile metals, damage models that have been traditionally developed relate failure strain to stress triaxiality, η, which is defined as the ratio between hydrostatic stress and equivalent stress. Bao and Wierzbicki [1-3] explored the effective plastic failure strain for a wide range of stress triaxialities. They reported that the effective plastic failure strain did not monotonically decrease with stress triaxiality. Likewise, Barsoum and Faleskog [4, 5] showed that the stress triaxiality alone is insufficient to properly describe the material behavior at failure. They introduced the Lode parameter μ to improve model accuracy and to properly describe the stress state. This parameter was based on the third invariant of stress tensor, as expressed in Eq. (1).

$$\mu = \frac{2\sigma_2 - \sigma_1 - \sigma_3}{\sigma_1 - \sigma_3},\tag{1}$$

where σ_1, σ_2, and σ_3 are the principal stresses.

In this sense, recent models consider the influence of the third invariant of deviator stress by the Lode parameter [6-11]. These models consider different geometries and stress conditions reported in the Refs. [1-11, 14-26]. They are included in Fig. 1 for the readers to identify the values of the stress triaxiality and the Lode parameter for each geometry. The main contributions for each study are included in Appendix A.

Bai et al. [6] and Gao et al. [8] predicted that stress triaxiality depended on specimen geometry and the plastic behavior of the material. They found that for materials that are weakly dependent on pressure and the Lode angle, such as 1045 steel or AA 5083-H116, the equivalent plastic strain decreased with an increase in stress triaxiality. In particular, for AA 5083-H116, Gao et al. [8] found that stress triaxiality had a relatively small effect on plasticity but had a significant effect on ductile failure strain. By contrast, the effect of the Lode angle on ductile fracture was negligible, but its effect on plasticity was significant.

In this regard, adequate damage models that link failure strain to stress triaxiality and the Lode parameter are necessary. In general, the calibration of these models has traditionally relied on specimens that exhibit high triaxiality and limited
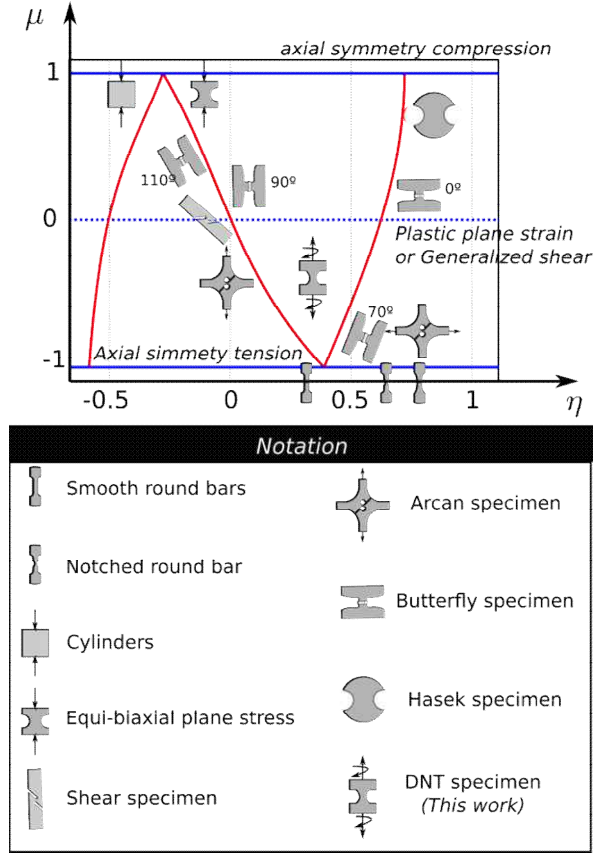
Fig. 1. Conceptual representation of the stress states on the plane of μ and η.

Fig. 2. Numerical model of DNT specimen.

Lode parameter.

This paper presents a procedure that combines tension and torsion to achieve different values of stress triaxiality (η) and Lode parameter (μ). For this objective, an experimental-numerical methodology based on the work of Barsoum and Faleskog for Weldox steel [4] is implemented for 2024-T3 aluminum, as shown in Appendix A. Experimental quasi-static tests and a numerical model are developed to obtain the relation between equivalent plastic failure strain and the stress state. The Double notched tube (DNT) specimen allows the achievement of low stress triaxiality and a range of Lode parameters in combined tension and torsion.

The fracture locus is constructed as a function of stress triaxiality and the third invariant of stress deviator, which confirms the combined void-shear nature of fracture.

2. Experimental test and set-up

The geometry of DNT is based on the specimen used by Barsoum and Faleskog for Weldox steel [4], which has not been previously applied for aluminum alloys. The dimensions of the DNT specimen are as follows: height H = 160 mm, exterior diameter d_{ext} = 24 mm, radius to the center of the notch r_m = 10.4 mm, and internal diameter of the tube d_{int} = 17.6 mm. The net section thickness at the notch is t_n = 1.2 mm
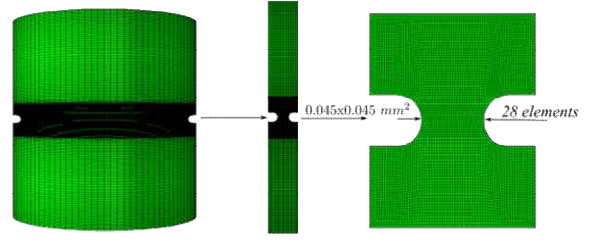
and the notch height is h = 1.0 mm. The tensile force N and the torsional moment M are applied at the end of the specimen, and the other one is clamped. The experiments are conducted using a Servosis ME-402 machine that is modified to achieve the combination of tensile force N and torsional moment M simultaneously, defined by loading parameter κ as follows:

$$\kappa = \frac{N \cdot r_m}{M} \ . \tag{2}$$

Combined tension-torsion tests are conducted in a range of loading parameter of $0.5 \le \kappa \le 7$, which corresponds to a tensile load from 0 kN to 80 kN and a torsion moment from 0 N·m to 600 N·m. This load combination provides stress triaxiality η from 0.1 to 1.2 in a range of Lode parameter of $-1 < \mu < 0$ at room temperature. Thirty-six specimens with the same geometry for different load conditions are used to perform this study. Both axial displacement and the rotation angle near the notch are monitored using a 3550HT axial/torsional extensometer from the Epsilon Technology.

3. Numerical analysis

The objective of the numerical model is to determine the stress triaxiality, Lode parameter, and equivalent plastic strain at failure times because the internal stress cannot be directly measured in experimental tests. The ABAQUS code is used to model the tension-torsion test and to evaluate the stress state over the notch. DNT specimen is modeled using four-node axisymmetric elements with twist (CGAX4R). The element size in the gauge section of both specimens is approximately 0.045 × 0.045 mm, as shown in Fig. 2.

The thermoviscoplastic behavior is defined by the Johnson-Cook plasticity model using the parameters from the works of Teng and Wierzbizcki and García-Gónzalez et al. [12, 29], as shown in Table 1.

The numerical results are compared with the experimental data in terms of force-displacement and torsional moment-rotation curves, as shown in Fig. 3.

The experimental and numerical curves are in good agreement, and thus, the numerical model is appropriately validated. The combined experimental and numerical methodology allows obtaining the stress and strain values in the notch region

Table 1. Properties of the 2024-T351 aluminum alloy [12, 29].

Elasticity	
$E(GPa)$	$\nu(-)$
70	0.3

Thermoviscoplastic behaviour					
$A(MPa)$	$B(MPa)$	$n(-)$	$\dot{\varepsilon}_0(s^{-1})$	$C(-)$	$m(-)$
352	440	0.42	$3.3\ 10^{-4}$	0.0083	1.7

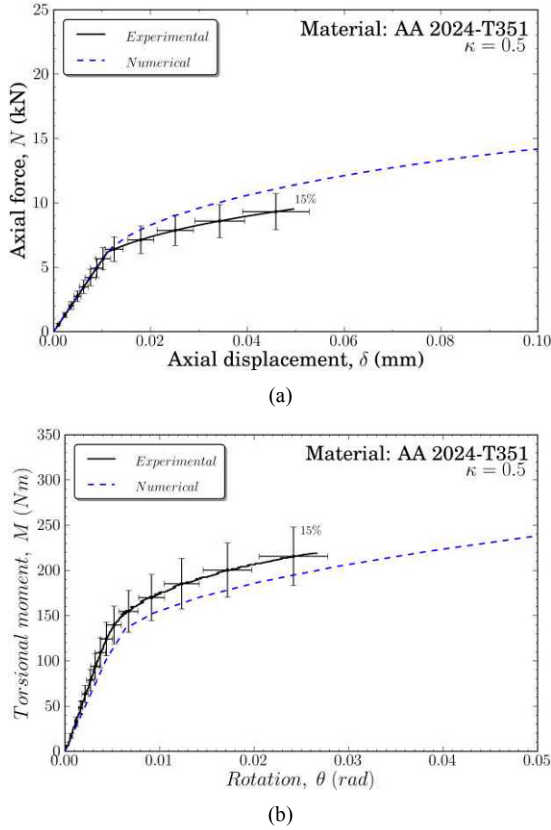| Other physical constants				
$\rho(kg/m^3)$	$\beta(-)$	$C_p(J/kg\,K)$	$T_0(K)$	$T_m(K)$
2700	0.9	900	293	775

(a)

(b)

Fig. 3. Comparison between the finite element simulations and the experimental results for the aluminum alloy 2024-T3 for κ = 0.5: (a) axial force versus axial displacement; (b) torsional moment versus rotation.

Fig. 4. Contour plot of plastic strain at failure, stress triaxiality, and Lode parameter in the notch region for different loading conditions.

of the specimen and therefore the relationship among failure equivalent strain, stress triaxiality, and Lode parameter.

4. Results

The DNT specimen used in the 2024-T3 aluminum provides adequate values of the displacement and rotation in the gauge section. The test is strongly stable in displacement-rotation control, and failure occurs close to the middle of the gauge se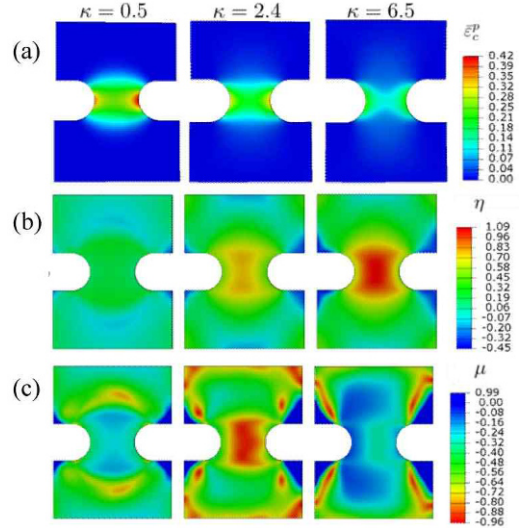ction. The numerical analysis reveals that the DNT specimen of 2024-T3 can be used to achieve values of stress triaxiality from 0.2 to 1.2 and values of Lode parameter from −1 to 0. Fig. 4(a) shows the localization of plastic strain, ε_p, in the notched region. This behavior agrees with the numerical results of other authors [2, 13]. In terms of stress triaxiality, η, the maximum values are observed in the notch center, and they decrease with the distance to the center, as shown in Fig. 4(b). Concerning the third invariant, the maximum numerical values of the Lode parameter, μ, also occur in the notch center, as shown in Fig. 4(c).

Therefore, the failure locus of the 2024-T3 aluminum is constructed in terms of stress triaxiality and Lode parameter (Fig. 5). Failure strain values are in good agreement with the numerical results of other works [11]; these values correspond to simple stress states, such as axisymmetric tension, plane stress tension, plane strain tension, and pure shear. The main advantage of the proposed methodology, however, is its capability of performing tests in a low-intermediate range of stress triaxiality using only one type of specimen (DNT specimen). This new methodology implies a significant simplification for the experimental analysis of failure.

According to the influence of the stress state, the results show that an increase in stress triaxialiaty values does not necessarily lead to a monotonic decrease in effective plastic failure strain values. This effect is explained by the rupture mechanisms associated with the ductile-fragile transition. For low values of stress triaxiality, the main failure model is the shear ductile rupture. The effective plastic strain increases with stress triaxiality up to a threshold value, μ = 0.68, which is a transition region where the main failure models are due to the shear ductile fracture and the internal void necking mechanism. The transition in the rupture mechanism is also observed for ductile steels [4]. Beyond this value of stress triaxiality, the effective plastic strain begins to decrease. The

Table 2. Constants of the calibration of the simplified Bai-Wierzbicki [7] for the aluminum alloy 2024-T3.

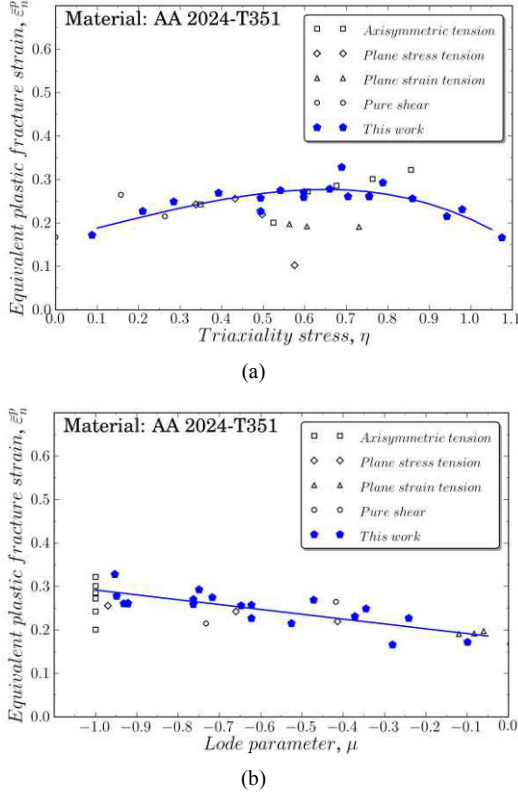|	
D_1	0.42
D_2	0.61
D_3	0.21
D_4	0.0013

(a)

(b)

Fig. 5. Fracture locus for the aluminum alloy 2024-T3 on the space of equivalent plastic strain versus: (a) stress triaxiality; (b) lode parameter.

global effect can be explained by the influence of the third invariant (Lode parameter). For high stress triaxiality values, the predominant failure mechanism is governed by void growth and coalescence. As stress triaxialiaty decreases, failure seems to change into shearing among voids. This behavior is not observed for metals that present weak dependency on the Lode parameter, such as 5083-H116 aluminum alloy [8] or DH36 steel [7], in which equivalent plastic strain decreases with increasing triaxiality without any change in the failure mechanism.

5. Calibration of damage model

The numerical-experimental methodology of this work provides adequate data for calibrating damage models. In this work, the constants for the simplified Bai-Wierzbicki [7] model for the aluminum alloy 2024-T3 are obtained according to Eq. (3) to obtain the failure strain, ε_f.

$$\varepsilon_f(\eta, \mu) = [D_1 \cdot e^{-D_2 \cdot \eta} - D_3 \cdot e^{-D_4 \eta}] \cdot \mu^2 + D_3 \cdot e^{-D_4 \eta}, \qquad (3)$$

where D_1, D_2, D_3, and D_4 parameters are presented in Table 2. This damage model is a useful tool for the accurate predictions of the failure of 2024-T3 aluminum structures.

6. Conclusions

Tensile-torsion tests are conducted on the aluminum alloy 2024-T3. A numerical-experimental methodology is successfully applied to the related failure strain to stress triaxiality and Lode parameter. The correlation between experimental and numerical simulations in the load-displacement response is satisfactory, with a maximum error of 10%. The maximum values of stress triaxiality are obtained in the notch center.

The main aspect of this work is the development of combined tension-shear tests using only one type of specimen (DNT). The use of the DNT specimen is proven to be efficient for calibrating a ductile failure model of aluminum alloys. The loading parameter can be modified to obtain a wide range of stress triaxiality and Lode parameter between the tension ($\mu = -1$) and shear ($\mu = 0$) in failure conditions. This procedure is satisfactorily used for the first time in the 2024-T3 aluminum alloy. The failure data that are obtained can be used to calibrate ductile fracture models. The Bai-Wierzbicki fracture model is also calibrated in this work.

Finally, the influence of the third invariant (Lode parameter) on AA 2024-T351 is proven, and the rupture mechanisms associated with the ductile-fragile transition are shown.

Nomenclature——————————————————————

N	: Axial force
M	: Torsional moment
δ	: Axial displacement
θ	: Rotation
σ	: Stress
ε_p	: Plastic strain
ε_f	: Failure strain
η	: Triaxiality stress
μ	: Lode parameter

References

[1] Y. Bao and T. Wierzbicki, *Prediction of ductile crack formation in uncracked bodies*, Massachussetts Institute of

Technology (2003).

[2] Y. Bao and T. Wierzbicki, On fracture locus in the equivalent strain and stress triaxiality space, *Int. J. Mech. Sci.*, 46 (2004) 81-98.

[3] Y. Bao, Dependence of ductile crack formation in tensile tests on stress triaxiality, stress and strain ratios, *Eng. Fracture Mech.*, 72 (4) (2005) 505-522.

[4] I. Barsoum and J. Faleskog, Rupture mechanisms in combined tension and shear—Experiments, *Int. J. Solids and Structures*, 44 (2007) 1768-1786.

[5] J. Faleskog and I. Barsoum, Tension-torsion fracture experiments—Part I: Experiments and a procedure to evaluate the equivalent plastic strain, *Int. J. Solids and Structures*, 50 (2013) 4241-4257.

[6] Y. Bai and T. Wierzbicki, A new model of metal plasticity and fracture with pressure and Lode dependence, *Int. J. Plasticity,* 24 (2008) 1071-1096.

[7] Y. Bai, X. Teng and T. Wierzbicki, On the application of stress triaxiality formula for plane strain fracture testing, *ASME J. Eng. Mater. Technol.,* 131 (2) (2009) 1-10.

[8] X. Gao, T. Zhang, M. Hayden and C. Roe, Effects of the stress state on plasticity and ductile failure of an aluminum 5083 alloy, *Int. J. Plasticity*, 25 (12) (2009) 2366-2382.

[9] X. Gao, G. Zhang and C. Roe, A study on the effect of the stress state on ductile fracture, *Int. J. Damage Mech.*, 19 (1) (2010) 75-94.

[10] G. Mirone and D. Corallo, A local viewpoint for evaluating the influence of stress triaxiality and Lode angle on ductile failure and hardening, *Int. J. Plasticity,* 26 (3) (2010) 348-371, doi:10.1016/j.ijplas.2009.07.006.

[11] J. D. Seidt, *Plastic deformation and ductile fracture of 2024-T351 aluminum under various loading conditions,* The Ohio State University (2010).

[12] X. Teng and T. Wierzbicki, Effects of fracture criteria on high velocity perforation of thin beams, *Int. J. Comput. Meth.*, 1 (2004) 171-200.

[13] J. Hancock and A. MacKenzie, On the mechanism of ductile failure in high-strength steels subjected to multi-axial stress-states, *J. Mech. Phys. Solids.*, 24 (1975) 147-169.

[14] J. Zhou, X. Gao, M. Hayden and J. A Joyce, Modeling the ductile fracture behavior of an aluminum alloy 5083-H116 including the residual stress effect, *Eng. Frac Mech.*, 85 (2012) 103-116, doi:10.1016/j.engfracmech.2012.02.014.

[15] H. Mae, X. Teng, Y. Bai and T. Wierzbicki, Ductile fracture locus of AC4CH-T6 cast aluminium alloy, *Archives of Computational Mat. Sci. and Surface Eng.,* 2 (2009) 100-105.

[16] M. Basaran, *Stress state dependent damage modeling with a focus on the lode angel influence*, Berichte aus dem Maschinenbau (2011).

[17] H. Li, M.W. Fu, J. Lu and H. Yang, Ductile fracture: Experiments and computations, *Int. J. Plasticity,* 27 (2) (2011) 147-180.

[18] J. Zhou, M. Hayden and X. Gao, An investigation of the strain rate and temperature effects on the plastic flow stress and ductile failure strain of aluminum alloys 5083-H116, 6082-T6 and a 5183 weld metal, *Proceedings of the Institution of Mechanical Engineers, Part C: J. Mech.l Eng. Sci.*, 0 (2012b) 1-13.

[19] J. Guo, S. Zhao, R. Murakami and S. Zang, Experimental and numerical investigation for ductile fracture of Al-alloy 5052 using modified Rousselier model, *Comp. Mat. Sci.,* 71 (2013) 115-123.

[20] M. Španiel, A. Prantl, J. Džugan, J. Ružička, M. Moravec and J. Kuželka, Calibration of fracture locus in scope of uncoupled elastic-plastic-ductile fracture material models, *Adv. Eng. Soft,* 72 (2014) 95-108.

[21] F. Ebnoether and D. Mohr, Predicting ductile fracture of low carbon steel sheets: Stress-based versus mixed stress/strain-based Mohr-Coulomb model, *Int. J. Solids and Structures,* 50 (7-8) (2013) 1055-1066.

[22] A. M. Beese, M. Luo, Y. Li, Y. Bai and T. Wierzbicki, Partially coupled anisotropic fracture model for aluminum sheets, *Eng. Frac. Mech.,* 77 (7) (2010) 1128-1152.

[23] M. Dunand and D. Mohr, On the predictive capabilities of the shear modified Gurson and the modified Mohr-Coulomb fracture models over a wide range of stress triaxialities and Lode angles, *J. Mech and Physics of Solids,* 59 (7) (2011) 1374-1394.

[24] M. Luo, M. Dunand and D. Mohr, Experiments and modeling of anisotropic aluminum extrusions under multi-axial loading - Part II: Ductile fracture, *Int. J. Plasticity,* (32-33) (2012) 36-58.

[25] T. Wierzbicki, Y. Bao and Y. Bai, New experimental technique for constructing a fracture envelope of metals under multi-axial loading, *Proceedings of the 2005 SEM Annual Conference and Exposition on Experimental and Applied Mechanics,* 1 (2005) 1295-1303.

[26] D. Mohr and S. Henn, Calibration of stress-triaxiality dependent crack formation criteria: A new hybrid experimental-numerical method, *Exp. Mech.,* 47 (6) (2007) 805-820.

[27] C. L. Walters, *Development of a punching technique for ductile fracture testing over a wide range of stress states and strain rates by*, Massachusetts Institute of Technology (2009).

[28] S. M. Graham, T. Zhang, X. Gao and M. Hayden, Development of a combined tension-torsion experiment for calibration of ductile fracture models under conditions of low triaxiality, *Int. J. Mech. Sci,.* 54 (1) (2012) 172-181.

[29] D. García-González, M. Rodríguez-Millán, A. Vaz-Romero and A. Arias, High impact velocity on multi-layered composite of polyether ether ketone and aluminium, *Comp. Interfaces,* 124 (2015) 705-715.

Appendix A

Table A.1. Summary of contributions of different authors to comparing different geometries.

Type of specimen	Test mode	Stress triaxiality (η)	Lode parameter (μ)	Material	Author	Year	Reference
Smooth round bars	Tension	$1/3$	-1	AA 2024-T351	Bao et al.	2003-2005	[1-3]
				AA 5083-H116	Gao et al Zhou et al.	2009 2012	[8] [14]
				AC4CH-T6 cast AA	Mae et al.	2009	[15]
				DP600 steel	Basaran	2011	[16]
				AA 6061-T6	Li et al.	2011	[17]
				AA 6082-T6	Zhou et al.	2012b	[18]
				AA 5052	Guo et al.	2013	[19]
				Austenitic Cr-Ni-Ti steel	Španiel et al.	2014	[20]
Notched round bar	Tension	$\frac{1}{3}+\sqrt{2}\cdot\ln\left(1+\frac{a}{2R}\right)$	-1	AA 2024-T351	Bao et al.	2003-2005	[1-3]
				AA 5083-H116	Gao et al. Zhou et al.	2009 2012	[8] [14]
				DH36 steel	Gao et al.	2010	[9]
				DP600 steel	Basaran	2011	[16]
				AA 6061-T6	Li et al.	2011	[17]
				AA 5052	Guo et al.	2013	[19]
				Low carbon steel	Ebnoether et al.	2013	[21]
				Austenitic Cr-Ni-Ti steel	Španiel et al.	2014	[20]
Plastic plane strain	Tension	$\frac{\sqrt{3}}{3}$	0	AA 2024-T351	Bao et al. Seidt	2003-2005 2010	[1-3] [11]
				AA 6061-T6	Beese et al. Li et al.	2010 2011	[22] [17]
				DP600 steel	Basaran	2011	[16]
				TRIP780 steel	Dunand et al.	2011	[23]
				AA 6260-T6	Luo et al.	2012	[24]
Flat grooved plates	Tension	$\frac{\sqrt{3}}{3}\left[1+2\ln\left(1+\frac{t}{4R}\right)\right]$	0	AA 2024-T351	Bao et al.	2003-2005	[1-3]
				AA 5083-H116	Gao et al Zhou et al.	2009 2012	[8] [14]
				DH36 steel	Gao et al.	2010	[9]
				AA 6061-T6	Beese et al.	2010	[22]
				DP600 steel	Basaran	2011	[16]
Torsion or	Torsion or shear	0	0	AA 2024-T351	Bao et al. Seidt	2003-2005 2010	[1-3] [11]
				AA 5083-H116	Gao et al. Zhou et al.	2009 2012	[8] [14]
				DH36 steel	Gao et al.	2010	[9]
				AA 6061-T6	Li et al.	2011	[17]
				AA 5052	Guo et al.	2013	[19]
Cylinders	Compression	$-\frac{1}{3}$	-1	AA 2024-T351	Bao et al. Seidt	2003-2005 2010	[1-3] [11]
				AA 6061-T6	Li et al.	2011	[17]
				AA 5083-H116	Zhou et al.	2012	[14]
Equi-biaxial plane stress	Tension	$\frac{2}{3}<\eta<0.83$	-1	AA 2024-T351	Bao et al.	2003-2005	[1-3]
Equi-biaxial plane stress	Compression	$-\frac{2}{3}<\eta<-0.35$	1	AA 2024-T351	Bao et al.	2003-2005	[1-3]

Type of specimen	Test mode	Stress triaxiality (η)	Lode parameter (μ)	Material	Author	Year	Reference
Plastic plane strain	Compression	$-\dfrac{\sqrt{3}}{3}$	0	AA 2024-T351	Bao et al.	2003-2005	[1-3]
				AA 6260-T6	Luo et al.	2012	[24]
Notched round bar	Compression	$-\left[\dfrac{1}{3}+\sqrt{2}\cdot\ln\left(1+\dfrac{a}{2R}\right)\right]$	1	AA 2024-T351	Bao et al.	2003-2005	[1-3]
				AA 6061-T6	Li et al.	2011	[17]
				AA 5083-H116	Zhou et al.	2012	[14]
Butterfly specimen	Biaxial	$-0.191 < \eta < 1.01$	-0.8 to 0.5	A710 steel	Wierzbicki et al.	2005	[25]
				Al-7Si-Mg alloy	Mohr et al.	2007	[26]
				DP600 steel	Walters Basaran	2009 2011	[27] [16]
				AC4CH-T6 cast AA	Mae et al.	2009	[15]
				AA 6061-T6	Beese et al.	2010	[22]
				TRIP780 steel	Dunand et al.	2011	[23]
				AA 6260-T6	Luo et al	2012	[24]
				Austenitic Cr-Ni-Ti steel	Španiel et al.	2014	[20]
Hasek specimen (Punch test)	Biaxial	$1/3 < \eta < 2/3$	$-0.6 < \eta < 1$	DP600 steel	Walters Basaran	2009 2011	[27] [16]
				AA 6061-T6	Li et al.	2011	[17]
				Austenitic Cr-Ni-Ti steel	Španiel et al.	2014	[20]
				Low carbon steel	Ebnoether et al.	2013	[21]
Lindholm specimen	Biaxial	$0 < \eta < 0.6$	$-1 < \mu < 0$	AA 5083.H116	Graham et al.	2012	[28]
DNT	Tension-torsion	$0.3 < \eta < 1.3$	$-1 < \mu < 0$	Weldox 420 steel Weldox 960 steel	Barsoum et al. Faleskog et al.	2007 2013	[4] [5]
				AA 2024-T351	*This work*		

Marcos Rodríguez-Millán received his doctoral degrees from the University Carlos III of Madrid, Spain in 2013. Dr. Rodríguez-Millán is an assistant professor at the Department of Mechanical Engineering of the University Carlos III of Madrid, Spain. His research interests are in the area of solid mechanics, dynamic problems, metals, and composites.